

Published in final edited form as:

J Pharm Pharmacol. 2012 November ; 64(11): 1592–1602. doi:10.1111/j.2042-7158.2012.01557.x.

EFFECT OF MICRONEEDLE TREATMENT ON THE SKIN PERMEATION OF A NANOENCAPSULATED DYE

Yasmine A. Gomaa [Assistant lecturer],

Department of Pharmaceutics, Faculty of Pharmacy, Alexandria University, El-Khartoum Square, Alexandria, 21521, Egypt. yasmine87ag@yahoo.com. Tel: +2- 01003409501, Fax: +2-03-4873273

Labiba K. El-Khordagui* [Professor],

Department of Pharmaceutics, Faculty of Pharmacy, Alexandria University, El-Khartoum Square, Alexandria, 21521, Egypt. lakhail@alexpharmacy.edu.eg. Tel: +2-0105550567, Fax: +2-03-4873273

Martin J. Garland [MPharm],

School of Pharmacy, Queen's University Belfast, Medical Biology Centre, 97 Lisburn Road, Belfast, BT9 7BL, UK. mgarland01@queens-belfast.ac.uk. Tel: +44 (0) 7725912704, Fax: +44 (0) 28 90 247 794

Ryan F. Donnelly [Senior Lecturer],

School of Pharmacy, Queen's University Belfast, Medical Biology Centre, 97 Lisburn Road, Belfast, BT9 7BL, UK. r.donnelly@qub.ac.uk. Tel: +44 (0) 28 90 972 251, Fax: +44 (0) 28 90 247 794

Fiona McInnes [Lecturer], and

Strathclyde Institute of Pharmacy and Biomedical Sciences (SIPBS), University of Strathclyde, 161 Cathedral Street, Glasgow, G4 0RE, UK. fiona.mcinnnes@strath.ac.uk, f.mcinnnes@dd-int.com. Tel: +44 (0)141 548 2506, Fax: +44 (0)141 552 2562

Victor M. Meidan [Lecturer]

Strathclyde Institute of Pharmacy and Biomedical Sciences (SIPBS), University of Strathclyde, 161 Cathedral Street, Glasgow, G4 0RE, UK. victor.meidan@strath.ac.uk, vmeidan@hotmail.com. Tel: +44 (0)141 548 4274, Fax +44 (0)141 5522562

Abstract

Objectives—The aim of the study was to investigate the effect of microneedle (MN) treatment on the transdermal delivery of a model drug (rhodamine B, Rh B) encapsulated in polylactic-co-glycolic acid (PLGA) nanoparticles (NPs) focusing on the MN characteristics and application variables.

Methods—Gantrez® MNs were fabricated using laser-engineered silicone micro-mould templates. PLGA NPs were prepared using a modified emulsion–diffusion–evaporation method

*Corresponding author.

Conflict of interest: The Author(s) declare(s) that they have no conflicts of interest to disclose.

and characterized *in vitro*. Permeation of encapsulated Rh B through MN treated full thickness porcine skin was performed using Franz diffusion cells using appropriate controls.

Key findings—*In vitro* skin permeation of the nanoencapsulated Rh B ($6.19 \pm 0.77 \mu\text{g}/\text{cm}^2/\text{h}$) was significantly higher ($P < 0.05$) compared to the free solution ($1.66 \pm 0.53 \mu\text{g}/\text{cm}^2/\text{h}$). Mechanistic insights were supportive of preferential and rapid deposition of NPs in the MN-created microconduits, resulting in accelerated dye permeation. Variables such as MN array configuration and application mode were shown to affect transdermal delivery of the nanoencapsulated dye.

Conclusions—This dual MN/NPs mediated approach offers potential for both the dermal and transdermal delivery of therapeutic agents with poor passive diffusion.

Keywords

Microneedles; nanoparticles; rhodamine B

Introduction

Microneedle (MN) array technology has attracted growing interest as a means of enhancing transdermal delivery of drugs in a minimally-invasive fashion [1] MN arrays consist of solid or hollow needles, ranging between 70 μm and 1000 μm in length, that are attached to a patch-like support [2-4]. When pressed into the skin, MNs breach the *stratum corneum*, forming microconduits that facilitate permeation of topically applied drugs. Upon MN removal, the inherent elasticity of skin tissue causes the pores to contract in a relatively short time [5, 6]. MN technology has been used to enhance skin permeation of numerous agents including; gold nanoparticles [7], drugs of diverse molecular weights [8-10], low molecular weight heparin [11], gene vectors [12], vaccines [13], therapeutic antibodies [14] and various nanocarriers [15, 16].

Combining MN treatment with another penetration enhancement method in order to enhance drug delivery has been the subject of several investigations. For instance MN treatment in conjunction with iontophoresis accelerated the transdermal delivery of various molecules, including; fluorescein isothiocyanate (FITC)-dextrans [17], methotrexate [18] and daniplestim [19]. Synergistically-enhanced flux of FITC-dextrans has also been achieved by combining MN use with 'in-skin' electroporation [20], while others have deployed MNs together with phospholipid vesicle systems and found it possible to enhance the *in vitro* penetration of mannitol [21] and docetaxel [15]. A sonophoretically-enhanced MN array method improved transdermal delivery rate of calcein and bovine serum albumin *in vitro* [22]. Interestingly, a triple enhancement strategy based on MN treatment, iontophoresis and nanovesicle-entrapped insulin was reported to allow efficacious transdermal drug delivery in diabetic rats *in vivo* [23].

Parallel with the developments in MN arrays, the design and development of engineered nanoparticles (NPs) as specialized drug carriers for percutaneous applications has also advanced. Such NP utilization may improve the skin retention of drugs allowing dose reduction, prolonged and / or enhanced release into skin and protection from enzymatic

degradation [16, 24]. However, the results of passive skin-NP interaction studies have been somewhat varied and contradictory [25-27]. There is an emerging consensus that NPs cannot usually penetrate the *stratum corneum*, although they may well deposit in hair follicles [28-31]. Clearly, precise behavior depends upon properties such as particle size, shape, composition, and charge, as well as the vehicular environment. Intuitively, it would seem that the insertion of MN into the skin followed by topical application of drug-loaded NPs should constitute a promising transdermal delivery approach. To date, most MN-NP combination studies have been aimed at achieving either transdermal vaccine delivery [13], transcutaneous immunization [32] and intradermal delivery of low molecular weight drugs using dissolving MNs [33]. Some research has been dedicated to uncovering the translocation and diffusion kinetics of unloaded NPs through MN-perforated skin [16, 34, 35].

The aim of the present study was to gain insight into the effect of MN treatment on the transdermal delivery of nanoencapsulated drugs. The permeation of a model fluorescent small/medium sized hydrophilic dye, Rhodamine B [36, 37], encapsulated in PLGA NPs was investigated using full thickness porcine skin. The influence of MN characteristics and application variables on the dye permeation was assessed.

Materials and methods

Chemicals

Gantrez® AN-139, a copolymer of methylvinylether and maleic anhydride, was a gift from ISP Co Ltd (Guildford, UK). Silastic® 9280/60E silicone elastomer was purchased from Dow Corning (Midland, MI). PLGA (Resomer RG 50:50 H; inherent viscosity 0.41 dl/g) was bought from Boehringer Ingelheim (Ingelheim, Germany). Didodecylmethyl ammonium bromide (DMAB), Rh B, trypan blue and phosphate buffer saline (PBS) tablets and hydrochloric acid (HCl) were obtained from Sigma-Aldrich (St. Louis, MO). Ethyl acetate (Fisher Scientific UK Ltd, Loughborough, UK), 'Silver dag' (Polysciences Inc., Eppelheim, Germany), Nanovan® (Nanoprobes®, Yaphank, NY, USA) and Shandon M-1 embedding OCT (optimal cutting temperature) matrix (Thermo Electron Corporation, UK) were also used.

Fabrication and imaging of MN arrays

Gantrez® AN-139 MN arrays with different needle lengths (400, 600, and 1000 µm) and MN densities (121, 196, and 361 MN/array) were fabricated using laser-engineered silicone micro-mould templates [1, 3]. For scanning electron microscopy (SEM) imaging (JSM 6400 digital scanning electron microscope, JEOL Ltd, Tokyo, Japan), arrays were mounted on aluminium stubs using double-sided adhesive tape and 'silver dag' and coated with gold/palladium (SC515 SEM sputter coater, Polaron, East Grinstead, UK).

Preparation and characterization of Rh B-loaded NPs

PLGA NPs were prepared using a modified emulsion-diffusion-evaporation method [38]. Briefly, the organic phase (2.5 mL ethyl acetate containing 50 mg PLGA 50:50) was homogenized with 200 µL distilled water at 15000 rpm for 5 min (Polytron PT4000, Switzerland). DMAB solution (5 mL 1% w/v aqueous solution) was added under stirring to

yield a w/o/w emulsion. Homogenization was continued at 15000 rpm for 5 min. The resulting emulsion was diluted (25 ml water) while stirring till separation of NPs. For Rh B-loaded NPs, 200 μ L of the dye solution (20% w/w) were used as aqueous phase for the primary emulsion.

For transmission electron microscope (TEM) imaging (LEO 912 AB, Cambridge, UK), 50 μ l volume of diluted NP suspension (1:10) was placed on the surface of a formvar/carbon coated 300 mesh grid and allowed to settle for 30 s. Nanovan® (5 μ l) was added and removed immediately. Grids were left to dry and then examined.

The size and Zeta potential of NPs, suspended in distilled water, were determined using a Nano ZS dynamic light scattering instrument (Malvern Instruments Ltd, Malvern, UK). The polydispersity index (PDI) was also obtained. Data are the mean of repeated measurements (five in case of size and 30 in case of Zeta potential) of three different batches.

Dye loading was determined spectrofluorimetrically [39] by measuring the fluorescence of a 300-fold diluted sample using a Varian Cary Eclipse Fluorescence spectrophotometer (Mulgrave, Victoria, Australia) at excitation and emission wavelengths 540 nm and 625 nm respectively.

Degradation of Rh B-loaded PLGA NPs dispersed in water and stored at 4°C, 25°C and 32°C over 7 weeks was assessed by monitoring pH lowering [40] using a microprocessor pH meter 211 (Hanna instruments, Leighton Buzzard, UK).

Skin permeation studies

Porcine ears (Landrace species), from a local abattoir, were harvested immediately following slaughter. Ears were sectioned using a scalpel to yield whole skin samples. The central part of the same ear was used to punch out skin samples for controls and tests. Skin was cut into circular samples (surface area of ~ 4 cm²) with average thickness 1164 ± 103 μ m (n = 46) measured with a digital micrometer. Full-thickness skins were wrapped in aluminum foil and stored at -80 °C for no longer than 6 months.

For MN insertion, skin samples were placed over a polystyrene foam support with *stratum corneum* uppermost. MN arrays were pressed down manually by the same operator, onto the centre of skin samples. For repeated insertions, arrays were rotated approximately 90° before each reinsertion.

Transepidermal water loss (TEWL) values were determined as reported [3, 41]. Skin samples were mounted in vertical Franz diffusion cells (PermeGear, Bethlehem, PA). Receiver phase was 5.3 mL PBS pH 7.4, stirred at 600 rpm at 37 ± 0.5 °C. TEWL was measured using AF103 AquaFlux® device (Biox Systems Ltd., London, UK) inserted into an empty donor cell secured over each skin sample. Initially, skins were left to hydrate in the cells for 1 h and then the donor cell microclimate was allowed to stabilize for 10 min. Data are means of several measurements taken over 5 min. After recording basal TEWL values, skin samples were removed and treated with 5 insertions of MN (600 μ m length, 121 MN/array) before re-mounting for subsequent measurements at 1, 2, 3 and 24 h.

In skin permeation experiments, skin samples were inserted into vertical Franz cells (diffusion area of 0.64 cm²) and left to equilibrate for 1 h. Donor chambers were loaded with 500 µL Rh B aqueous control solution or Rh B-loaded NP dispersion in water with similar dye content under non-occlusive conditions. Receiver compartments were filled with 5.3 mL PBS, pH 7.4 at 37°C stirred at 600 rpm. Samples (100 µL) of receiver compartment were removed over 48 h and replaced with an equal volume of fresh PBS. Rh B was assayed spectrofluorimetrically and data corrected for receiver phase dilutions. At 48 h, samples of receiver buffer were examined by TEM for possible translocation of NPs across the skin. The same procedure was used to screen the effects of four MN treatment parameters, namely MN length (400, 600 and 1000 µm), array density (121, 196 and 361 MN/array), number of insertions (1, 5 and 9) and insertion duration (2 s, 3 min and 5 min), on Rh B permeation. All experiments were run at least in triplicate. At the end of the permeation experiment, skin samples were embedded in OCT medium and cryosectioned using a Shandon Cryotome® SME Cryostat (Fisher Thermo Scientific, Asheville, NC) to produce 10 µm-thick vertical skin sections. These were imaged using DFC320 camera and light microscope system (Leica Microsystems Wetzlar GmbH, Germany).

Two additional control permeation experiments were undertaken. The first involved a longer equilibration period (2 h) of MN-treated skin prior to exposure to Rh B-loaded NPs dispersion to test the effect of pore closure with time on dye permeation. The second involved exposing the MN-treated skins to Rh B dissolved in a dispersion of blank PLGA NPs to assess possible effect of residual surfactant (DMAB) in the NP dispersion on the skin permeation of Rh B.

Breaching of the *stratum corneum* by MNs of different dimensions and application variables was visualized using trypan blue staining (0.4% w/v in PBS (pH 7.4)) of the *stratum corneum* side of MN-treated skins for 1 h. The dye was then washed off under cold water. *Stratum corneum* and dermal sides were examined and photographed using a 12.2 megapixel Samsung digital camera (Shanghai, China).

Statistical analysis

Student's unpaired t-test was performed on permeation data at $P < 0.05$ using Minitab 16 statistical software (Minitab Inc., State College, PA, USA).

Results

Microneedle arrays

Microneedles (MN) and MN arrays with different MN densities fabricated in the study are shown in Figure 1a and Figure 1b-d, respectively. MNs were conical in shape with a base width of 300 µm.

PLGA NPs properties

Figure 2 shows TEM images of the Rh B-loaded NPs. These were spherical with a fairly uniform size. The size, PDI and Zeta potential of obtained NPs were 105 ± 2.92 nm, 0.15 ± 0.02 and 55 ± 2.86 mV, respectively. The loading capacity of Rh B NP dispersion was 77.54

$\pm 3.14 \mu\text{g/mL}$ and its pH was 3.2. An aqueous solution of Rh B of the same concentration and pH (adjusted using 0.1 M HCl) was used as control in permeation experiments.

Possible *in vitro* degradation of Rh B-PLGA NPs dispersion (pH 3.24 ± 0.02 , $n=9$) was investigated by measuring the decrease in pH of the dispersion over a 7 week-study period at 3 different temperatures. Figure 3 shows the derived pH versus time plots. No measurable change in pH of NP dispersions, particularly those kept at 4°C and ambient temperature (25°C), was noted. However, at 32°C, a progressive decrease in pH was observed to start after about one week.

Skin permeation studies

Prior to conducting the skin permeation experiments, the integrity of skin samples and the formation and closure of MN-created microconduits were assessed by TEWL measurements. Results are shown in Figure 4. Obtained basal TEWL value for untreated full thickness porcine skin ($29.4 \pm 2.6 \text{ g / m}^2 \text{ h}$) was in good agreement with values previously reported [41]. Post MN treatment, TEWL significantly ($P < 0.01$) increased so as to produce a mean peak of $56.4 \pm 8 \text{ g / m}^2 \text{ h}$ at 1 h. This was followed by a slow decline in TEWL reaching approximate basal values at 24 h ($30.8 \pm 4.8 \text{ g / m}^2 \text{ h}$). This decline can be explained by closure of MN-created skin pores over time [3, 21].

Figure 5 shows the effect of MN treatment and / or nanoencapsulation on the skin permeation of Rh B across full thickness porcine skin for 48 h. In these experiments, each MN treatment consisted of 5 repeat insertions of arrays exhibiting 600 μm -long MNs at a density of 121 MN/array left in place for 2 seconds after last insertion. In experiments involving NPs, these could not be detected by TEM in the receiver compartments at 48 h. All cumulative dye permeation profiles (Figure 5) showed a lag time with negligible dye permeation corresponding to the dye accumulation in skin samples [15]. Lag times were shorter for permeation of the encapsulated dye. It can be seen that lag times in these plots tended to be an appreciable fraction of the total 48 h permeation period, which may influence reliability of quantitative steady state flux values. Given this, flux values were supported with data for total amount permeated per unit area at 24 and 48 hrs expressed as Q (in $\mu\text{g/cm}^2$), and percent of Rh B that permeated the skin at 48 h. Data are presented in Table 1.

Quantitative skin permeation data shown in Figure 5 and Table 1 were qualitatively reinforced with light microscopic visualization of histologically sectioned skin samples. Vertical section photomicrographs are shown in Figure 6. Exposure of untreated skin samples to free Rh B control solution resulted in localization of the dye (pink coloration) in the *stratum corneum* and viable epidermis (Figure 6(a)). Puncturing of skin samples with MN prior to application of Rh B control solution created microchannels that protruded as finger-like projections into the upper layers of the porcine dermis (Figure 6(b)). These channels infiltrated by the dye solution, were typically more than 100 μm deep and $\sim 30\mu\text{m}$ wide, although dimensional distortions created as an artifact of the embedding and sectioning processes cannot be excluded. Nanoencapsulation of Rh B appeared to enhance the dye permeation, as indicated by the intense staining of the epidermis and diffusion to deeper skin layers (Figure 6(c)). Crucially, the combination of Rh B nanoencapsulation and

skin treatment with MN produced the greatest apparent dye infiltration into deeper skin layers (Figure 6(d)). Figures 6 (e) and (f) showed preferential accumulation of the dye in hair follicles of untreated skin exposed to the Rh B NP dispersion.

Figure 7 shows the results of two additional control experiments involving the effect of post-MN insertion equilibration time (1 vs 2 h) and the possible effect of residual amounts of surfactant (DMAB) used in NP preparation on the skin permeation of nanoencapsulated Rh B. It could be noted that the cumulative amount of Rh B permeated at 48 h was significantly ($P = 0.018$) reduced when equilibration time was doubled. Concerning a possible surfactant enhancing effect on dye permeation, data were obtained for skin samples treated with MN under similar conditions and exposed either to a control dye solution or blank NP dispersion in the control dye solution. Q_{48} value for the dye solution containing blank NPs was not significantly different ($P = 0.283$) from that of the control dye solution but was significantly ($P < 0.00005$) lower than that for Rh B loaded NP dispersion (Figure 7). This excludes a possible surfactant enhancing effect and lends support to a nanoencapsulation enhancing effect.

The influence of the MN parameters related to characteristics and application variables on the transdermal delivery of nanoencapsulated Rh B was investigated using untreated skin as control. Insertion of arrays having MN lengths of 400 and 600 μm resulted in flux values of 2.37 ± 0.62 and $6.19 \pm 0.77 \mu\text{g}/\text{cm}^2/\text{h}$ and mean Q_{48} of 1.63 ± 0.43 and $5.40 \pm 0.39 \mu\text{g}/\text{cm}^2$, respectively.

A further increase in MN length (1000 μm) did not significantly increase Rh B flux ($7.10 \pm 0.22 \mu\text{g}/\text{cm}^2/\text{h}$, $P = 0.19$) or Q_{48} ($5.71 \pm 0.06 \mu\text{g}/\text{cm}^2$, $P = 0.3$). For the effect of MN array density, application of the 121 MN/ array produced a flux of $6.19 \pm 0.77 \mu\text{g}/\text{cm}^2/\text{h}$ and a mean Q_{48} value of $5.40 \pm 0.39 \mu\text{g}/\text{cm}^2$. These values were not significantly increased by increasing MN density to 196 MN/ cm^2 (flux $6.65 \pm 0.22 \mu\text{g}/\text{cm}^2/\text{h}$, mean Q_{48} $5.43 \pm 0.18 \mu\text{g}/\text{cm}^2$). Nevertheless, a further increase in MN density to 361 MN/ cm^2 actually significantly reduced dye delivery, yielding a flux of $5.08 \pm 0.34 \mu\text{g}/\text{cm}^2/\text{h}$ and mean Q_{48} of $5.44 \pm 0.16 \mu\text{g}/\text{cm}^2$.

One, five and nine insertion(s) resulted in average flux of $6.38 \pm 0.42 \mu\text{g}/\text{cm}^2/\text{h}$, $6.19 \pm 0.77 \mu\text{g}/\text{cm}^2/\text{h}$, and $7.47 \pm 0.14 \mu\text{g}/\text{cm}^2/\text{h}$, respectively. This corresponds to average Q_{48} values of $4.55 \pm 0.20 \mu\text{g}/\text{cm}^2$, $5.40 \pm 0.39 \mu\text{g}/\text{cm}^2$ and $6.05 \pm 0.21 \mu\text{g}/\text{cm}^2$ respectively.

Differences between flux and Q_{48} values obtained at different multiple insertions were not statistically significant. In tests of skin insertion duration, it was found that insertion periods of 2 s, 3 min and 5 min yielded fluxes of $6.19 \pm 0.77 \mu\text{g}/\text{cm}^2/\text{h}$, $5.51 \pm 0.05 \mu\text{g}/\text{cm}^2/\text{h}$ and $5.20 \pm 0.37 \mu\text{g}/\text{cm}^2/\text{h}$ which corresponds to mean final dye amounts of 5.40 ± 0.39 , 3.80 ± 0.06 and $3.69 \pm 0.25 \mu\text{g}/\text{cm}^2$ respectively which were not statistically different.

Each of the distinct MN treatments described above was also screened by means of trypan blue staining which confirmed perforation of the *stratum corneum*, indicating adequate sharpness of all MNs (figures not shown). No blue spots were seen on the dermal side of the skin at 1 h indicating inability of even the longest MN to create holes that would extend through the full thickness of the skin.

Discussion

MN arrays were successfully prepared with different needle lengths and densities as confirmed by SEM. MN tips were sharp enough to breach the *stratum corneum* as evident from Figures 6(b) and (d), appearance of trypan blue spots (figures not shown) and TEWL measurements (Figure 4). Rh B NPs were monodisperse (PDI < 0.2) and colloidally stable (zeta potential > 30 mV) [42].

One interesting feature of this study involved the results obtained from passive permeation experiments (i.e. no MN application). Namely, it was found that in comparison to application of free Rh B solution, application of Rh B-loaded NPs resulted in an approximately nine-fold increase in dye permeating across full thickness porcine skin. When contemplating this seemingly counterintuitive result, it is important to note that NPs were thermally-stable for 48 h at the temperatures encountered in the Franz cell system. However, we did find some visual evidence of preferential NPs deposition in the hair follicles as shown in Figures 6(e) and (f). Porcine ear infundibula are reported to show a diameter of approximately 200 μm [43]. Infiltration of PLGA NPs carrying their dye payload may be mediated by the medium lipophilicity inside the hair follicles [44] and the polymer hydrophobicity. Once deposited in the hair follicles, the absence or immaturity of the *stratum corneum* in these locations [28] would allow Rh B released from the NPs to laterally diffuse into the viable epidermis. This mechanism explains the results of this study - namely enhancement of transdermal dye delivery combined with an absence of NPs in the receiver solution. Unfortunately, visualization of individual NPs using techniques such as confocal microscopy was not feasible in our study due to their small size which was below the resolution limit [45, 46]. Yet this idea of preferential localization of NPs in follicles is supported by literature findings [16, 29, 30, 47]. For example, Lademann's group [29] reported preferable deposition of PLGA NPs (320 nm) into porcine hair follicles *in vitro*. Rancan and colleagues [30] observed *in vitro* penetration of polylactic acid fluorescent NPs (228 and 365 nm) into 50% of available vellus hair follicles. Benson's group [47] showed that PLGA NPs tended to deposit around follicles and sebaceous glands of human skin *in vitro*. Recent imaging of PLGA NPs (160, 200 and 288 nm) indicated their ready follicular penetration when applied to full-thickness human skin [16].

As might be expected, skin puncturing with MN arrays accelerated the transdermal permeation of free Rh B through the newly created pores acting as microchannels. However, of even greater interest was the fact that MN treatment followed by Rh B-loaded NPs resulted in an even greater transdermal delivery of Rh B. This is explainable by the newly created microchannels acting as additional preferred residing sites for loaded NPs (Figure 6(d)). Rh B released from these NPs would be able to freely diffuse laterally into the permeable tissues underlying the cornified layer, allowing accelerated dye transdermal delivery. Similar findings involving faster skin permeation of a drug loaded into a carrier relative to the free drug have been reported [15, 21, 48].

The reason for choosing the Q_{48} as an additional tool for comparison was based on the observation that the difference in permeation between the dye solution and the encapsulated dye became more statistically significant with time (24 vs 48 h) (Table 1). This was in

agreement with the observation of Zhang *et al.*, 2010 [16] who showed that the percentage of the applied NPs deposited in the epidermis and in the dermis in the MN-treated human skin increased more rapidly than that in the control groups over time. This implies that the advantage of using MN to enhance the intradermal delivery of NPs would be greater by time. Porcine skin barrier function proved to be maintained for 48 h using TEWL measurements [49].

It seems that the dye-loaded NPs rapidly flow into the microconduits created by the MNs. These pore-residing NPs act as dye depots, releasing Rh B directly into the deeper skin layers. The fact that increasing the post-MN treatment equilibration time reduced permeation strongly supports the concept of the preferential accumulation of NPs into those pores. This trend can be explained in terms of a 2 h (TEWL = $45.4 \pm 5 \text{ g / m}^2 \text{ h}$) period allowing greater contraction of the MN-generated skin defects than a 1 h period (TEWL = $56.4 \pm 8 \text{ g / m}^2 \text{ h}$). This type of mechanism is also consistent with the reports of others, such as the visualized confinement of PLGA NPs to the entire length of MN-created pores in human skin [16].

Another aim of the current study was to investigate how the MN-NP dual approach for transdermal dye delivery could be modulated with different MN characteristics and application variables. With respect to MN length, insertion of 600 μm -long needles was significantly more permeabilizing than insertion of 400 μm -long needles, but use of the 1000 μm long needles did not yield further significant increase. Such a pattern of direct correlation between needle length and permeabilization below a threshold MN length has been observed before [8]. It is explainable in terms of the increased frictional resistance encountered by the longest needles [50]. This is due to these structures exhibiting a greater needle to skin contact surface area. Longer MNs may require a greater insertion force to be applied in order for their use to be effective. Indeed, different threshold needle length values have been reported by various groups [7, 13, 20]. In terms of MN density, the highest tested density of needles per array was actually less effective than lower densities. This is thought to be due to the so called 'the bed of nails' effect. This is where the pressure exerted by each needle tip can be reduced to a potentially insufficient level to penetrate as deeply into skin as an array of lower density when the same force is spread over a very large number of needles [2, 51-53]. With respect to the number of array insertions, our studies indicated that more insertions resulted in greater transdermal permeation of the model dye. This is consistent with the idea that the more MN insertions, the more microconduits are created in the *stratum corneum*. Furthermore, there is some evidence from a previous TEWL-based study that partial pore reclosure may be somewhat suppressed when skin poration is very high [3]. This can be attributed to the progressive increase difficulty for the skin to effectively contract and reduce the pore sizes as the number of channels increases [3]. The duration of MN skin insertion is another important variable and the present study suggests that this should be kept brief. One explanation for this effect is thought to be due to the accelerated elastic contractions caused by the prolonged embedding of the MNs in the tissue resulting in partially closing of many MN-induced conduits. The same observation for the effect of prolonged MN insertion on the barrier function and hence permeability was previously reported using dermatomed human skin (DHS) as monitored by TEWL

measurements^[3]. Leaving the array in the DHS for several minutes partially suppressed the fall of barrier function at 1 h. More investigations are now required in order to elucidate the precise details of this proposed mechanism. Those results were also in accordance with those obtained by Yong's group^[4] where they showed insignificant increase in the permeability of galanthamine when MN insertion time exceeded 1 min in rat skin.

Conclusions

We have provided new knowledge on the MN-driven skin permeation of a small / medium-sized molecular weight model compound loaded in polymer NPs. A MN insertion and nanoencapsulation dual approach can be used to enhance transdermal delivery across full thickness porcine skin. The principal impact of this research stems from the counter-intuitive result that dye loaded-NPs can deliver greater transdermal dye permeation than that from a free dye solution. This is probably due to a mechanism of preferential NP deposition in hair follicles and microchannels combined with good lateral diffusion kinetics of the free compound. Further investigation is clearly needed for a better mechanistic understanding of the 3-way interactions of polymeric NPs with MN created skin channels and encapsulated dye. This will allow optimization of the dual enhancement approach for possible transdermal applications of controlled drug delivery.

Acknowledgments

Funding: This work was supported by the Egyptian Channel Programme. The development of the laser engineering method for MN manufacture by Queen's University of Belfast was supported by the Biotechnology and Biological Science Research Council [Grant no: BBE020534/1] and Invest Northern Ireland [Grant no: PoC21A].

6. References

1. Donnelly RF, et al. Microneedle-based drug delivery systems: microfabrication, drug delivery, and safety. *Drug Deliv.* 2010; 17:187–207. [PubMed: 20297904]
2. Verbaan FJ, et al. Improved piercing of microneedle arrays in dermatomed human skin by an impact insertion method. *J Control Release.* 2008; 128:80–88. [PubMed: 18394741]
3. Gomaa YA, et al. Effects of microneedle length, density, insertion time and multiple applications on human skin barrier function: assessments by transepidermal water loss. *Toxicol In Vitro.* 2010; 24:1971–1978. [PubMed: 20732409]
4. Wei-Ze L, et al. Super-short solid silicon microneedles for transdermal drug delivery applications. *Int J Pharm.* 2010; 389:122–129. [PubMed: 20096759]
5. Gupta J, et al. Kinetics of skin resealing after insertion of microneedles in human subjects. *J Control Release.* 2011; 154:148–155. [PubMed: 21640148]
6. Kalluri H, Banga AK. Formation and closure of microchannels in skin following microporation. *Pharm Res.* 2011; 28:82–94. [PubMed: 20354766]
7. Kim CS, et al. Efficient and facile delivery of gold nanoparticles in vivo using dissolvable microneedles for contrast-enhanced optical coherence tomography. *Biomed Opt Express.* 2010; 1:106–113. [PubMed: 21258450]
8. Verbaan FJ, et al. Assembled microneedle arrays enhance the transport of compounds varying over a large range of molecular weight across human dermatomed skin. *J Control Release.* 2007; 117:238–245. [PubMed: 17196697]
9. Banks SL, et al. Transdermal delivery of natrexol and skin permeability lifetime after microneedle treatment in hairless guinea pigs. *J Pharm Sci.* 2010; 99:3072–3080. [PubMed: 20166200]
10. Mikolajewska P, et al. Microneedle pre-treatment of human skin improves 5-aminolevulinic acid (ALA)- and 5-aminolevulinic acid methyl ester (MAL)-induced PpIX production for topical

- photodynamic therapy without increase in pain or erythema. *Pharm Res.* 2010; 27:2213–2220. [PubMed: 20676735]
11. Lanke SS, et al. Enhanced transdermal delivery of low molecular weight heparin by barrier perturbation. *Int J Pharm.* 2009; 365:26–33. [PubMed: 18801420]
 12. Coulman SA, et al. Minimally invasive cutaneous delivery of macromolecules and plasmid DNA via microneedles. *Curr Drug Deliv.* 2006; 3:65–75. [PubMed: 16472095]
 13. Bal SM, et al. Microneedle-based transcutaneous immunisation in mice with n-trimethyl chitosan adjuvanted diphtheria toxoid formulations. *Pharm Res.* 2010; 27:1837–1847. [PubMed: 20559701]
 14. Lia G, et al. In vitro transdermal delivery of therapeutic antibodies using maltose microneedles. *Int J Pharm.* 2009; 368:109–115. [PubMed: 18996461]
 15. Qiu Y, et al. Enhancement of skin permeation of docetaxel: a novel approach combining microneedle and elastic liposomes. *J Control Release.* 2008; 129:144–150. [PubMed: 18538885]
 16. Zhang W, et al. Penetration and distribution of PLGA nanoparticles in the human skin treated with microneedles. *Int J Pharm.* 2010; 402:205–212. [PubMed: 20932886]
 17. Wu XM, et al. Enhancement of skin permeation of high molecular compounds by a combination of microneedle pretreatment and iontophoresis. *J Control Release.* 2007; 118:189–195. [PubMed: 17270306]
 18. Vemulapalli V, et al. Synergistic effect of iontophoresis and soluble microneedles for transdermal delivery of methotrexate. *J Pharm Pharmacol.* 2008; 60:27–33. [PubMed: 18088502]
 19. Katikaneni S, et al. Molecular charge mediated transport of a 13 kD protein across microporated skin. *Int J Pharm.* 2009; 378:93–100. [PubMed: 19501142]
 20. Yan K, et al. Transdermal drug delivery by in-skin electroporation using a microneedle array. *Int J Pharm.* 2010; 397:77–83. [PubMed: 20619329]
 21. Badran MM, et al. Skin penetration enhancement by a microneedle device (Dermaroller®) in vitro: Dependency on needle size and applied formulation. *Eur J Pharm Sci.* 2009; 36:511–523. [PubMed: 19146954]
 22. Chen B, et al. Sonophoretic enhanced microneedles array (SEMA)—Improving the efficiency of transdermal drug delivery. *Sensors and Actuators B: Chemical.* 2010; 145:54–60.
 23. Chen H, et al. Iontophoresis-driven penetration of nanovesicles through microneedle-induced skin microchannels for enhancing transdermal delivery of insulin. *J Control Release.* 2009; 139:63–72. [PubMed: 19481577]
 24. Prow TW, et al. Nanoparticles and microparticles for skin drug delivery. *Adv Drug Deliv Rev.* 2011; 63:470–491. [PubMed: 21315122]
 25. Tinkle S, et al. Skin as a route of exposure and sensitization in chronic beryllium disease. *Environ Health Persp.* 2003; 111:1202–1208.
 26. Kohli AK, Alpar HO. Potential use of nanoparticles for transcutaneous vaccine delivery: Effect of particle size and charge. *Int J Pharm.* 2004; 275:13–17. [PubMed: 15081134]
 27. Shim J, et al. Transdermal delivery of mixnoxidil with block copolymer nanoparticles. *J Control Release.* 2004; 97:477–84. [PubMed: 15212879]
 28. Meidan VM, et al. Transfollicular drug delivery--is it a reality? *Int J Pharm.* 2005; 306:1–14. [PubMed: 16260102]
 29. Lademann J, et al. Nanoparticles-An efficient carrier for drug delivery into the hair follicles. *Eur J Pharm Biopharm.* 2007; 66:159–164. [PubMed: 17169540]
 30. Rancan F, et al. Investigation of polylactic acid (pla) nanoparticles as drug delivery systems for local dermatotherapy. *Pharm Res.* 2009; 26:2027–2036. [PubMed: 19533305]
 31. Wu X, et al. Disposition of nanoparticles and an associated lipophilic permeant following topical application to the skin. *Mol Pharm.* 2009; 6:1441–1448. [PubMed: 19630400]
 32. Kumar A, et al. Permeation of antigen protein-conjugated nanoparticles and live bacteria through microneedle-treated mouse skin. *Int J Nano Med.* 2011; 2011:1253–1264.
 33. Donnelly RF, et al. Microneedle-mediated intradermal nanoparticle delivery: Potential for enhanced local administration of hydrophobic pre-formed photosensitisers. *Photodiag Photodyn Ther.* 2010; 7:222–231.

34. Coulman SA, et al. Microneedle mediated delivery of nanoparticles into human skin. *Int J Pharm.* 2009; 366:190–200. [PubMed: 18812218]
35. Park JH, et al. A microneedle roller for transdermal drug delivery. *Eur J Pharm Biopharm.* 2010; 76:282–289. [PubMed: 20624460]
36. Guss R, et al. Rhodamine B as a test molecule in intraocular dynamics. *Invest Ophthalmol Vis Sci.* 1984; 25:758–762.
37. Merck. [4.11.2010] Safety Data Sheet. www.merck-chemicals.com
38. Mittal G, et al. Estradiol loaded PLGA nanoparticles for oral administration: effect of polymer molecular weight and copolymer composition on release behavior in vitro and in vivo. *J Control Release.* 2007; 119:77–85. [PubMed: 17349712]
39. Kuchler S, et al. Influence of nanocarrier type and size on skin delivery of hydrophilic agents. *Int J Pharm.* 2009; 377:169–172. [PubMed: 19439166]
40. Contreras, JEL., et al. Human skin drug delivery using biodegradable PLGA – nanoparticles [dissertation]. University of Saarland; Saabruken: 2007.
41. Elmahjoubi E, et al. Transepidermal water loss for probing full-thickness skin barrier function: correlation with tritiated water flux, sensitivity to punctures and diverse surfactant exposures. *Toxicol In Vitro.* 2009; 23:1429–1435. [PubMed: 19577629]
42. Sugrue S. Predicting and controlling colloid suspension stability using electrophoretic mobility and particle size measurements. *Am Lab.* 1992; 24:64–71.
43. Jacobi U, et al. Porcine ear skin: an in vitro model for human skin. *Skin Res Technol.* 2007; 13:19–24. [PubMed: 17250528]
44. Nicolaidis N, et al. The skin surface lipids of man compared with those of eighteen species of animals. *J Invest Dermatol.* 1968; 51:83–89. [PubMed: 4980329]
45. Egner, A.; Hell, SW. Aberrations in confocal and multi-photon fluorescence microscopy induced by refractive index mismatch. In: Pawley, JB., editor. *Handbook of Biological Confocal Microscopy.* Springer Science Business Media; New York: 2006. p. 404-413.
46. Heilemann M. Fluorescence microscopy beyond the diffraction limit. *J Biotechnol.* 2010; 149:243–251. [PubMed: 20347891]
47. Wang F, et al. Formulation of nano and micro PLGA particles of the model peptide insulin: Preparation, characterization, stability and deposition in human skin. *Open Drug Deliv J.* 2008; 2:1–9.
48. Wang Q, et al. Improved dermal delivery of FITC-BSA using a combination of passive and active methods. *J Pharm Sci.* 2011; 100:4804–4814. [PubMed: 21721004]
49. Milewski M, et al. In vitro permeation of a pegylated naltrexone prodrug across microneedle-treated skin. *J Control Release.* 2010; 146:37–44. [PubMed: 20678989]
50. Martanto W, et al. Mechanism of fluid infusion during microneedle insertion and retraction. *J Control Release.* 2006; 112:357–361. [PubMed: 16626836]
51. Teo AL, et al. Transdermal microneedles for drug delivery applications. *Mater Sci Eng: B.* 2006; 132:151–154.
52. Bal SM, et al. Advances in transcutaneous vaccine delivery: Do all ways lead to Rome? *J Control Release.* 2010; 148:266–282. [PubMed: 20869998]
53. Yan G, et al. Evaluation needle length and density of microneedle arrays in the pretreatment of skin for transdermal drug delivery. *Int J Pharm.* 2010; 391:7–12. [PubMed: 20188808]

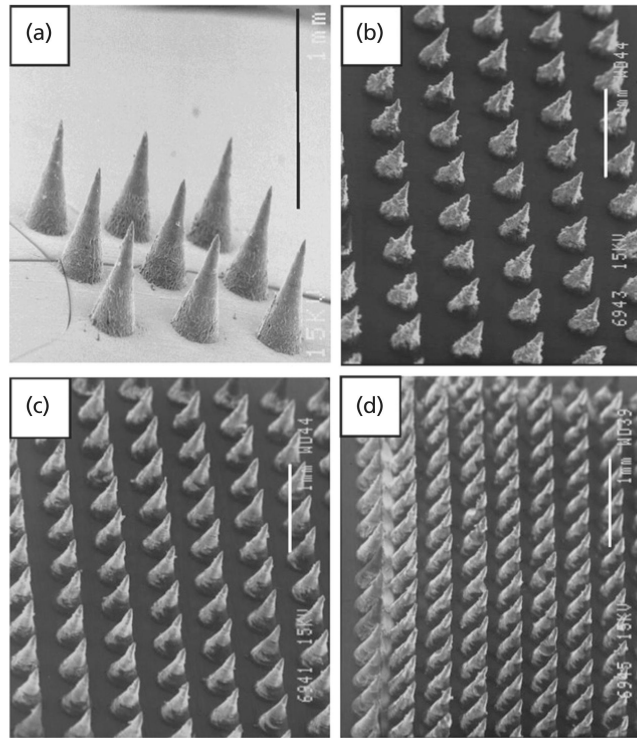


Figure 1. Fabricated arrays of 600- μ m-long microneedles (MNs) as viewed by scanning electron microscopy.

(a) Individual MNs. Arrays exhibiting 121 MNs (b), 196 MNs (c) and 361 MNs (d). Bar scales represent 1 mm.

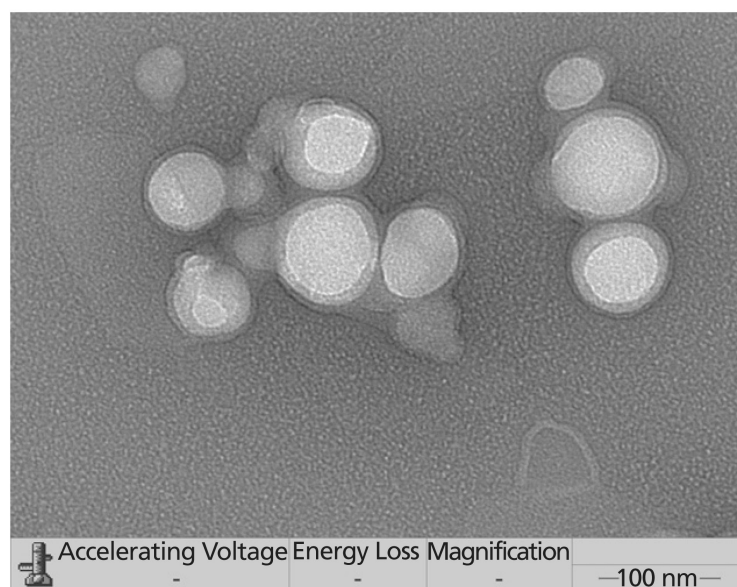


Figure 2. Transmission electron microscopy image of Rh B-loaded nanoparticles (magnification 40,000 \times).

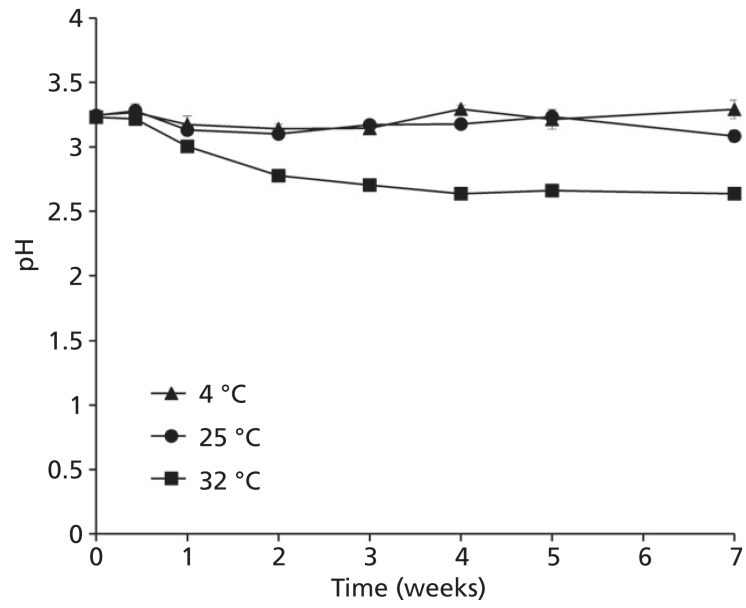


Figure 3. pH vs time plots for polylactic-co-glycolic acid nanoparticle aqueous dispersions incubated at three different temperatures.
Data are presented as mean \pm SD, $n = 3$.

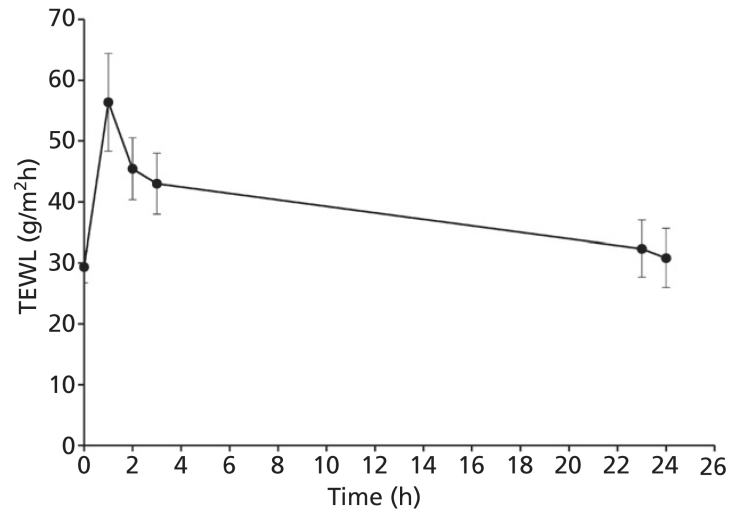


Figure 4. Trans-epidermal water loss (TEWL) of full-thickness microneedle-treated porcine skin determined using AquaFlux.

Data are presented as mean \pm SD, $n = 3$.

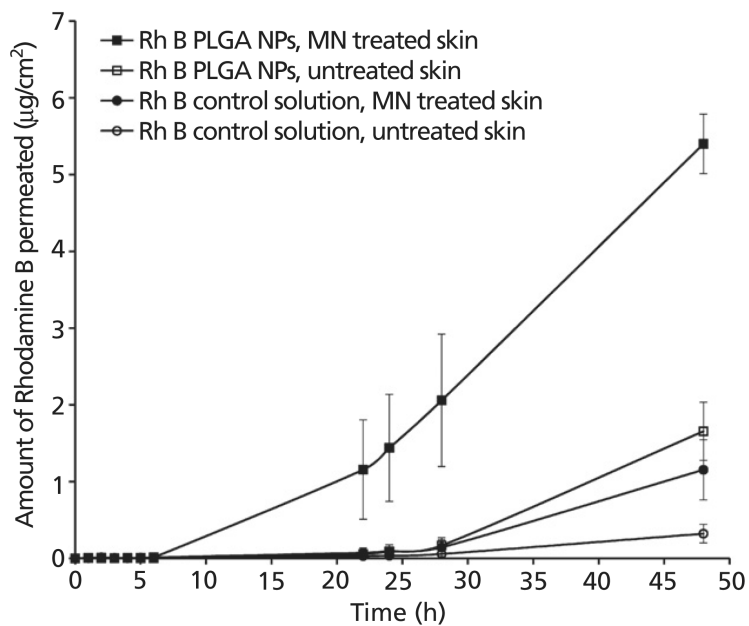


Figure 5. The influence of microneedle treatment and/or nanoencapsulation on the cumulative transdermal permeation of Rhodamine B. MN, microneedle; NP, nanoparticle; RhB, Rhodamine B; PLGA, polylactic-coglycolic acid. Data are presented as mean \pm SD, $n = 3$.

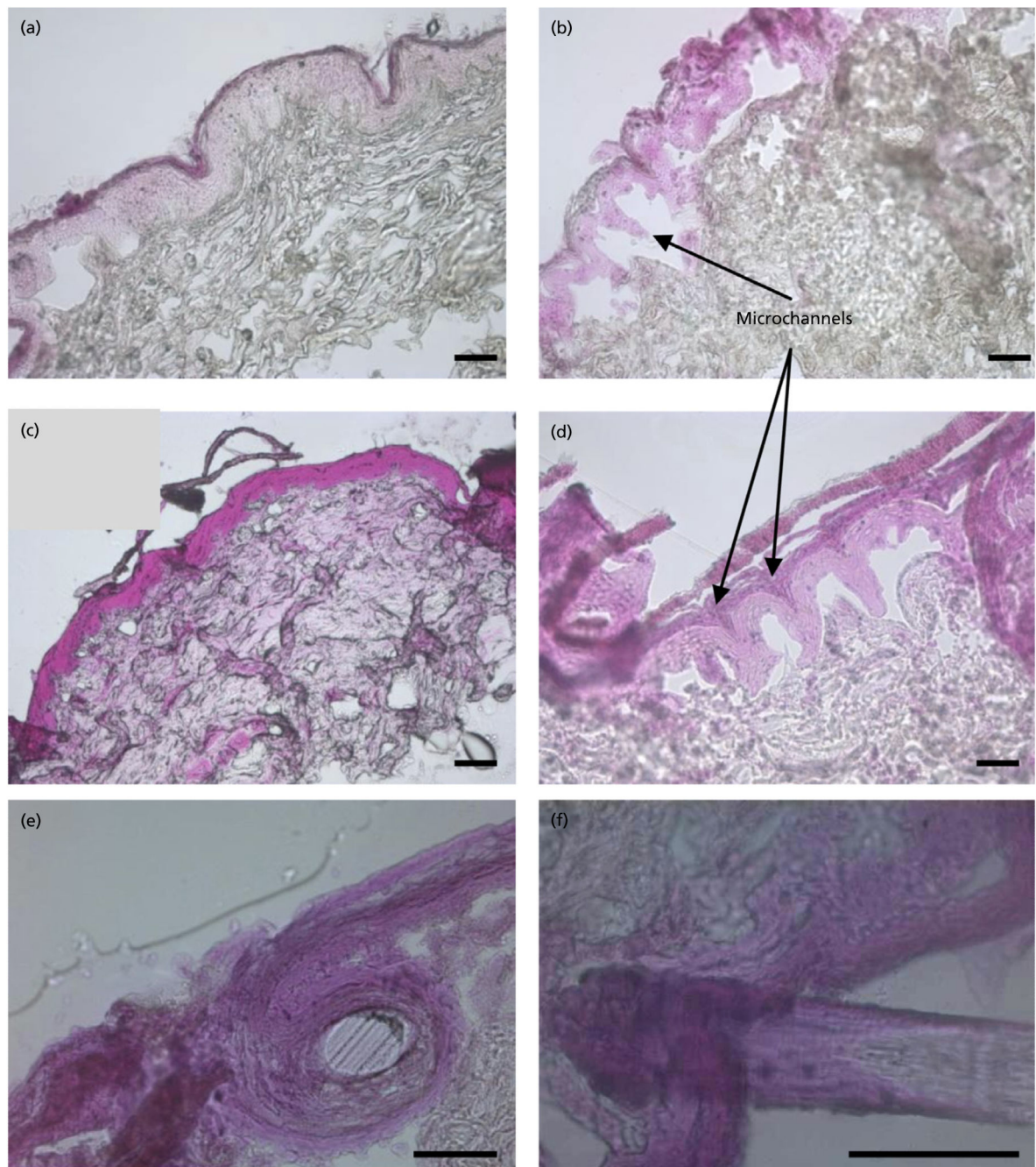


Figure 6. Light microscopy images showing the influence of microneedle (MN) treatment and/or dye nanoencapsulation on Rhodamine B (Rh B) ingress into porcine skin.

(a) Free dye with no MN treatment. (b) MN treatment followed by application of free dye. (c) Nanoencapsulated dye with no MN treatment (d) MN treatment followed by application of nanoencapsulated dye. (e and f) Accumulation of Rh B dye in the hair follicles of untreated porcine skin exposed to Rh B NPs. Bar scales represent 100 μm .

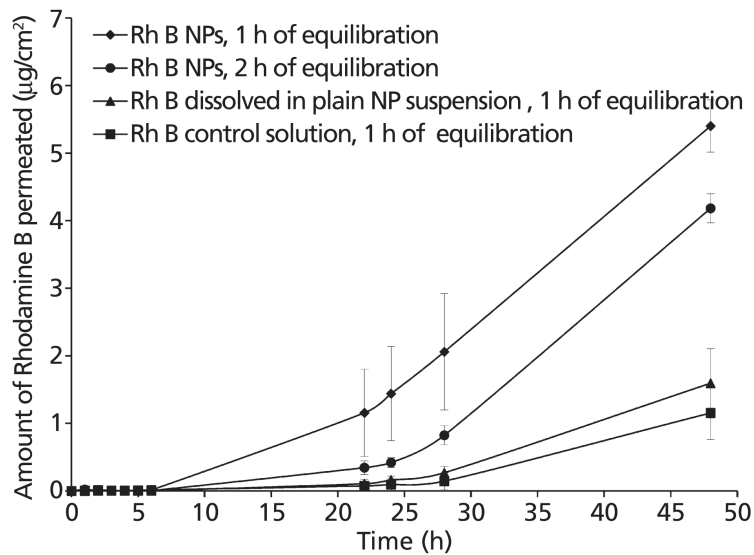


Figure 7. Cumulative permeation of Rhodamine B (Rh B) across porcine skin upon application of Rh B-loaded poly(lactic-co-glycolic acid) nanoparticles (NPs) following 1 h and 2 h equilibration time and upon application of Rh B dye dissolved in a dispersion of blank NPs following 1 h equilibration time in comparison with a dye solution of equal concentration.

Data are presented as mean \pm SD, $n = 3$.

Table 1
Statistical analysis showing the effect of nanoencapsulation on the permeation of Rh B through untreated and MN treated full thickness porcine skin.

Values are averages \pm SD (n = 3).

	Q ₂₄ ($\mu\text{g}/\text{cm}^2$)	P-value	Q ₄₈ ($\mu\text{g}/\text{cm}^2$)	P-value	% Penetration at 48 h	P-value	Steady state flux ($\mu\text{g}/\text{cm}^2/\text{h}$)	P-value
Untreated skin								
Rh B control solution	0.03 \pm 0.02	0.076	0.32 \pm 0.12	0.000*	0.53 \pm 0.20	0.000*	0.45 \pm 0.16	0.000*
Rh B NP suspension	0.09 \pm 0.06		1.66 \pm 0.38		2.73 \pm 0.62		2.44 \pm 0.53	
MN treated skin								
Rh B control solution	0.09 \pm 0.08	0.080	1.15 \pm 0.39	0.000*	1.90 \pm 0.64	0.000*	1.66 \pm 0.53	0.012
Rh B NP suspension	1.44 \pm 0.70		5.40 \pm 0.39		8.91 \pm 0.64		6.19 \pm 0.77	

* < 0.00005